Journal of Computer-Aided Molecular Design
https://doi.org/10.1007/s10822-020-00306-0

Characterization of PD-L1 binding sites by a combined FMO/GRID-DRY approach

Roberto Paciotti[1] · Mariangela Agamennone[1] · Cecilia Coletti[1] · Loriano Storchi[1,2]

Received: 14 October 2019 / Accepted: 9 March 2020

Abstract

The programmed cell death protein 1 (PD-1) and its ligand, PD-L1, constitute an important co-inhibitory immune checkpoint leading to downregulation of immune system. Tumor cells developed a strategy to trigger PD-1/PD-L1 pathway reducing the T cell anticancer activity. Anti-PD-L1 small drugs, generally with improved pharmacokinetic and technological profiles than monoclonal antibodies, became an attractive research topic. Nevertheless, still few works have been published on the chemical features of possible binding sites. In this work, we applied a novel computational protocol based on the combination of the ab initio Fragment Molecular Orbital (FMO) method and a newly developed GRID-DRY approach in order to characterize the PD-L1 binding sites, starting from PD-1/PD-L1 and PD-L1/BMS-ligands (Bristol–Mayers Squibb ligands) complexes. The FMO method allows the calculation of the pair-residues as well as the ligand–residues interactions with ab initio accuracy, whereas the GRID-DRY approach is an effective tool to investigate hydrophobic interactions, not easily detectable by ab initio methods. The present GRID-DRY protocol is able to determine the energy contributions of each ligand atoms to each hydrophobic interaction, both qualitatively and quantitatively. We were also able to identify the three specific hot regions involved in PD-1/PD-L1 protein–protein interaction and in PD-L1/BMS-ligand interactions, in agreement with preceding theoretical/experimental results, and to suggest a specific pharmacophore for PD-L1 inhibitors.

Keywords PD-1/PD-L1 · FMO · GRID-DRY · Protein–protein interactions · Hydrophobic interactions · PD-L1 inhibitors

Abbreviations

BMS	Bristol–Mayers Squibb
DRY	Hydrophobic probe
E_{es}	Electrostatic energy
E_{ex}	Exchange repulsion energy
E_{ct}	Charge transfer energy
E_{disp}	Dispersion energy
E_{solv}	Solvation energy
EEL	Electrostatic energy
EHB	Hydrogen-bonding energy
ELJ	Lennard–Jones energy
ES	Entropic energy
FMO	Fragment molecular orbitals
G	Region on PD-L1 surface delimited by Asp26, Asp122, Tyr123, Lys124 and Arg125
HE	Hydrophobic interaction energy
HOP	Hybrid orbital projection
HTRF	Homogenous time resolved fluorescence
MAO	Mechanism of action
MIFs	Molecular interaction fields
N1	Neutral flat N–H probe
O	Carbonyl oxygen probe
OH2	Water molecule probe
PCM	Polarizable continuum model
PD-1	Programmed cell death protein 1
PDB	Protein data bank
PD-L1	Programmed cell death protein 1 ligand
PIE	Pair interaction energy
PIEDA	Pair interaction energy decomposition analysis
PPI	Protein–protein interaction
P1	Region on PD-L1 surface composed of Tyr56, Glu58, Arg113, Met115 and Tyr123

Electronic supplementary material The online version of this article (https://doi.org/10.1007/s10822-020-00306-0) contains supplementary material, which is available to authorized users.

✉ Roberto Paciotti
r.paciotti@unich.it

✉ Loriano Storchi
loriano@storchi.org

[1] Department of Pharmacy, Università "G. D'Annunzio" Di Chieti-Pescara, Chieti, Italy

[2] Molecular Discovery Limited, Middlesex, London, UK

Published online: 17 March 2020

P2	Region on PD-L1 surface composed of Met115, Ala121 and Ty123
QSAR	Quantitative structure−activity relationship
R^2	Squared Pearson's correlation coefficient
RI-MP2	Second-order Møller–Plesset perturbation theory (MP2) gradient with resolution of the identity (RI) approximation
3D	Three-dimensional
SAR	Structure–activity relationship

Introduction

Over the last years the study of new pharmaceutical compounds able to interact with the immune system has become an important research area for discovering new anticancer drugs. Although cancer cells can be recognized and killed by the immune system, tumors have developed many immune evasion strategies such as the secretion of immunosuppressive factors and down regulation of crucial surface proteins (e.g. MHC class I) [1]. In particular, one of these strategies consists of the activation of inhibitory receptors (also called immunologic checkpoints) in immune cells, like the programmed death receptor 1 (PD-1). In normal conditions, PD-1 and the PD-1 inhibitory receptor ligand (PD-L1) are involved in the self-tolerance by suppressing the T cell activity. Their overexpression on tumor cells leads to a suppression of antigen-specific T cell response with consequent general immune dysfunction [1]. Much effort has thus been made to find useful strategies in immunologic checkpoint blockade. Promising results were found by utilizing monoclonal antibodies (mAbs): mAbs can interact with the PD-1 receptor on immune effector cells or with PD-L1 on tumor cells, leading to a reduction of cancer-induced immunosuppression [2, 3].

Nivolumab [4] and pembrolizumab [5] are two mAbs binding to PD-1, approved for the treatment of metastatic melanoma but other mAbs are enrolled in clinical studies. In many tumors like melanoma, ovarian, and lung cancers, PD-L1 is overexpressed on tumor cell [6, 7]. This evidence suggested a useful alternative cancer therapy using antibodies that bind PD-L1, instead of PD-1. Indeed, as a further benefit, several approved mAbs inhibiting PD-L1 (Atezolizumab, Durvalumab and Avelumab) have been hypothesized to possess less immune-related toxicity than anti-PD-1 therapy, partially because of the selectivity of the immune response in the tumor microenvironment [8–12].

Although mAbs therapy demonstrated good results, some disadvantages affect the use of antibody drugs, as the high production cost, difficulties in manufacture, stability, immunogenicity and lack of oral bioavailability. For this reason the research of new small-molecule inhibitors acting on PD-1, and its ligand, PD-L1, has recently become an important research topic in drug discovery [13–15].

The first library of small ligands binding PD-L1 was patented by Bristol-Myers Squibb (BMS) whose ligands are characterized by a (2-methyl-3-biphenylyl)methanol scaffold [16–18]. In order to clarify their mechanism of action, several crystal structures of PD-L1 with BMS inhibitors have been resolved by Holak and co-workers (PDB code: 5J89, 5J8O, 5N2F, 5N2D, 6R3K and 5NIU) [19–21]. X-ray results indicate that new molecules bind specifically PD-L1 and not PD-1, demonstrating that the goal to disrupt PD-1/PD-L1 can be also reached by the use of small molecules. Moreover, the analysis of X-ray structures revealed that the characteristic (2-methyl-3-biphenylyl)methanol scaffold is involved in hydrophobic interactions leading to the dimerization of PD-L1 [20, 21]. Since the first disclosure of these small binders, several libraries of non-peptide small-molecule disruptors of PPI of PD-1/PD-L1 were patented. One of them refers to molecules with the 1,3,4-oxadiazole and 1,2,4-thiadiazole moieties, currently in phase 1 of clinical trials [22]. Many other small-molecule inhibitors based on peptidomimetics [23–25] or macrocyclic peptides [26–28] were also reported, proving that the overall inhibition of the PD-1/PD-L1 interaction is a possible and promising therapeutic approach for cancer immunotherapy [29].

Complete and exhaustive descriptions of state of art of peptide and small molecule inhibitors on PD-1/PD-L1 have been recently proposed by Chen et al. and by Guzik et al. [12, 30]. Nevertheless, no published data are available concerning their mechanism of action or their specific target.

The discovery of new small-molecule disruptors of PD-1/PD-L1 interaction falls in the fascinating but also difficult and challenging research area of inhibition of protein–protein interaction (PPI) [31–33]. This is due to the particular nature of protein–protein interface, which is typically large, flat and flexible where only few residues are crucial for PPI, called "hot spots", generally surrounded by energetically less important amino acids, as suggested by the "O ring" theory [34–36].

In this picture, computational methods can play an important role to support rational drug design and many approaches were used in order to improve the identification of druggable hot spots and then hot regions, like "Robetta" and the "Presaging Critical Residues in Protein interfaces-Web Server" (PCRPi-W), just to cite some of them [37–40].

Among ab initio computational methods, Fragment Molecular Orbital approach [41–43] demonstrated to be a powerful tool to investigate protein–protein, DNA–protein and ligand–protein interactions as well as the stability of protein structures (intradomain and interdomain interactions) [44–48]. Moreover, the FMO method was already applied on PD-1/PD-L1 and PD-L1/ligands complexes,

showing to be an effective approach for accessing this particular system [49, 50].

The discovery of PD-L1 inhibitors with a low molecular weight has only recently begun [13] and a limited number of research articles has been published concerning their specific mechanism of action (MOA). Therefore, little information is available to the scientific community, limiting the development of new research studies aimed to detect new drug entities targeting PD-L1 protein.

In the present work, in order to identify key features characterizing the pharmacophore model of anti-PD-L1 small drugs we applied the FMO method to PD-1/PD-L1 heterodimer (PDB code: 4ZQK) and to PD-L1/BMS-ligands (PDB code: 5J89, 5J8O, 5N2F, 5N2D, 6R3K and 5NIU). Moreover, with the aim to enhance our results and forecasts, considering that ab initio methods fail to evaluate hydrophobic interactions and that this type of interaction plays a critical role in PPIs, we will illustrate a new application of the GRID DRY probe [51] that can be a powerful tool to highlight all hydrophobic spots.

The coupled FMO/GRID approach allowed us to identify the specific hydrophobic interactions as well as the specific electrostatic contacts involving the PD-L1 residues, detected in both PD-1/PD-L1 and PD-L1/BMS-ligands complexes.

Methods

FMO calculations

All structures analyzed in this report were obtained from Protein Data Bank (PDB). The complex with PDB code 4ZQK is the X-ray structure of the heterodimer PD-1/PD-L1 [52]. In the following, the residues of PD-L1 protein are indicated by adding the subscript L to the name of the residue (e.g. $_{L}$Tyr123). The other six structures investigated here, PDB codes 5J8O, 5J89, 5N2F, 5N2D, 5NIU and 6R3K, describe the complex between small molecule ligands and the dimerized form of the PD-L1 protein. These pdb files present a pair of dimers as the crystal unit (chains A/B and C/D). Before starting our computational procedure a single dimer from each pdb file was selected and aligned to PD-L1_chain A/BMS ligand/PD-L1_chain B of 6R3K pdb file. So, we refer to subunit A as the chain of dimer aligned to 63RK chain A and to subunit B as the protein unit aligned to 6R3K chain B.

After removing the explicit water molecules, the pdb structures were refined by Protein Preparation Wizard [53, 54] and possible missing side chains were filled by Prime [54–56]. Then, all refined structures were minimized by Macromodel with OPLS3e force field and PRCG minimization method using the "gradient" convergence criterion [54]. The protonation state of ligands was determined by LigPrep, at pH 7 ± 2 [53].

Single-point energy calculations were carried out over such refined geometries by using the ab initio fragment molecular orbital (FMO) method at the RI-MP2/6-31G level of theory, implemented in the GAMESS-US program package, adopting the PCM < 1 > method to describe the solvation effect [42, 57–63].

The minimized structures used for FMO calculations were fragmented into single amino acid residues for both PD-L1 and PD-1 proteins, with the exception of residues involved in disulfide-bond as Cys40–Cys114 and Cys54–Cys123 which were considered as a single fragment. The fragmentation point was located between Cα and NH group, using the hybrid orbital projection (HOP) treatment for bond detachment. FMO method allows calculating the pair interaction energy (PIE^{IJ}) between any pair of fragments I and J. The PIE value can be divided into five energy components by applying the pair interaction energy decomposition analysis (PIEDA) [64, 65], as shown by the following equation:

$$PIE^{IJ} = E_{es} + E_{ex} + E_{ct} + E_{disp} + E_{solv} \quad (1)$$

where the terms E_{es}, E_{ex}, E_{ct}, E_{disp} and E_{solv} refer respectively to electrostatic, exchange repulsion, charge transfer, dispersion and solvation energies. These terms are particularly useful to investigate the nature of ligand–protein interaction and to establish which energy component plays the main role in the binding process. E_{es} component is related to Coulomb interaction between charged or polarized fragments. The E_{ex} term is always repulsive and can be ascribed to steric repulsion between close fragments. The E_{ct} component is related to the interaction between occupied orbitals of a donor and unoccupied orbitals of an acceptor. The dispersion energy term, E_{disp}, takes into account the contribution of the interaction between the temporary dipole moments of two fragments, especially important for residues not exposed to the solvent and involved in the hydrophobic interactions [66]. On the other hand, if the hydrophobic interaction is manly related to a desolvation process (entropic contribution) the E_{disp} term cannot properly describe all the hydrophobic energy, leading to underestimate the contribution to the total interaction energy of such hydrophobic residues. Finally, E_{solv} describes the solvation energy.

In the present work, all the PIE values between each PD-L1 residue and PD-1 protein, and vice versa, were collected in order to detect the main residues involved in PD-1/PD-L1 interaction. The PIE values can be plotted versus the number of the interacting protein fragments, revealing the key interactions as the most negative bands. This representation is particularly useful to analyze similar systems as well as the interactions occurring between several ligands and a specific protein.

In order to evaluate the reliability of FMO results, Alascan calculations were also performed on the 4ZQK minimized structures by means of the Robetta software [37].

For ligand–protein complexes, FMO calculations were performed twice: i) considering ligands as a whole and ii) fragmenting each ligand in three or four sub-units, according to their characteristic functional groups, as summarized in Fig. 1.

In particular, ligands **3**, **4**, **5** and **6** were split up in three fragments: fragment **a** contains the biphenyl moiety; **b** contains one aromatic ring connected to a biphenyl group by an O atom, and fragment **c**, characterized by the presence of an amide group and one/two charged groups. Ligands **1** and **2** are characterized by a fourth fragment, **d**, represented in both cases by the benzonitrile moiety. For all ligands the fragmentation points were chosen so not to disrupt the aromatic systems, and to maintain the different ligand moieties separated, as reported in Fig. 1.

The total PIEs between ligands and each PD-L1 residue have been calculated and the results have been summarized in a PIE graph.

When the ligand is split, each fragment is denoted as $\mathbf{L_n}$, where **n** indicates the specific moiety included in that fragment as previously reported.

Each PIE value computed between $\mathbf{L_n}$ and the PD-L1 residues describes the interaction of a specific ligand moiety with any protein residue, thus providing useful information about the binding motif.

Amino acids belonging to subunits A or B are identified adding A or B to the residue name (e. g. $_A$Tyr123).

The total PIE was correlated to the experimental pIC_{50} obtained by means of the homogenous time resolved fluorescence (HTRF) assay [16]. Specifically, for ligand

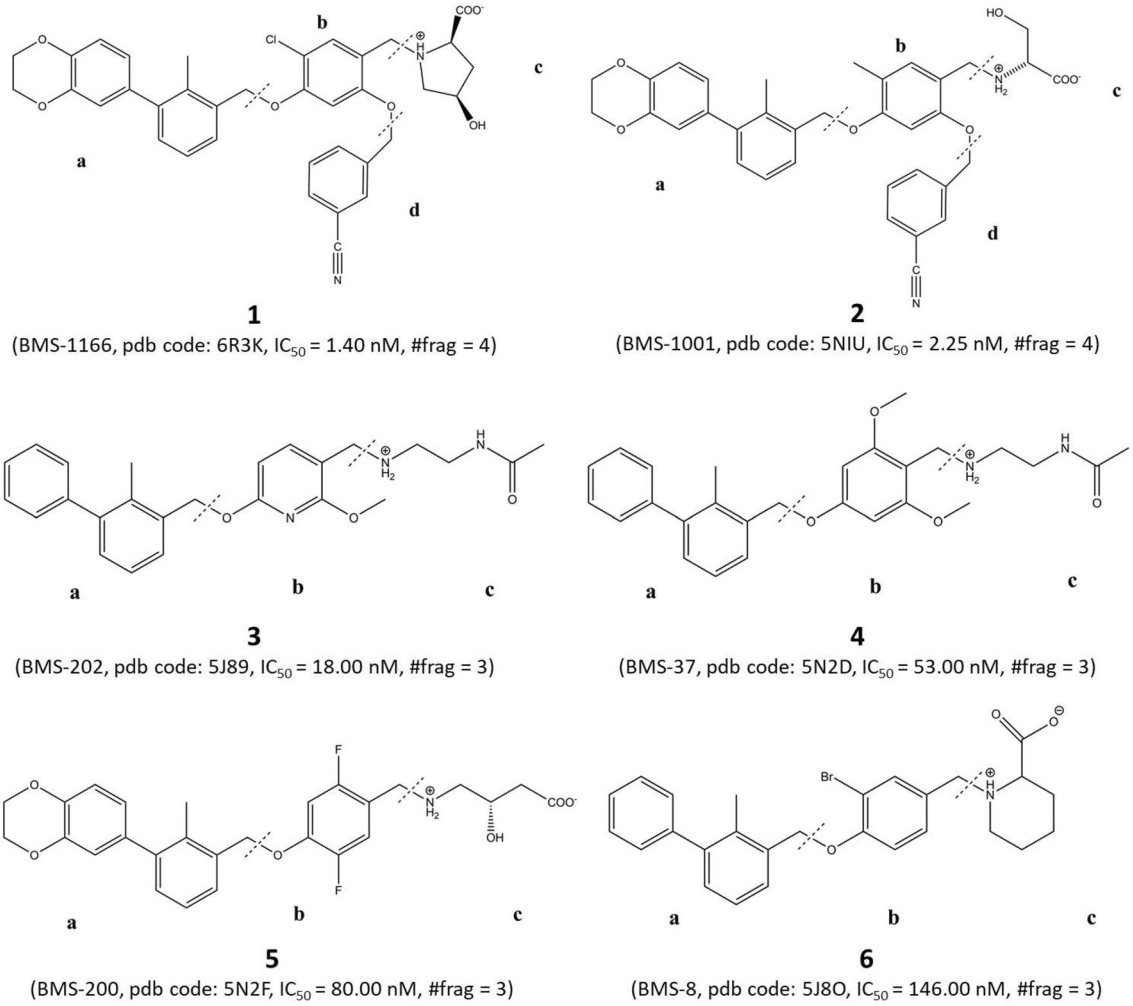

Fig. 1 Structure of the BMS-ligands investigated in this work. For each structure the patent ID code, the PDB code of the corresponding PD-L1/BMS-ligand complex, the number of ligand fragments (#frag), the protonation state and the experimental IC_{50}, obtained by means of HTRF binding assay, are reported. The fragmentation points are indicated by a dashed line and each fragment is indicated with a letter, from **a** to **d**

3 (BMS-37, PDB code 5N2D), a range of activity of 6–100 nM has been reported so that for that ligand an intermediate value of 53 nM was used in our correlation study.

GRID calculations

The GRID MIFs (i.e. GRID molecular interaction fields) [51, 67], originally developed for structure-based drug design [68], have been applied to a variety of drug discovery areas over the years, such as pKa [69] and tautomers modelling [70], scaffold-hopping [71, 72], 3D-QSAR [73], and metabolism prediction [74]. Using the GRID MIFs one can easily obtain information related to non-covalent bonding between the selected probe and the target. The target may either be a small molecule or a protein. Probes, on the other hand, represent different chemical moieties (e.g. OH2 a water molecule, DRY the hydrophobic probe, N1 a neutral flat N–H, O a carbonyl oxygen, etc.) that are located in a 3D grid surrounding the target. At each point of the 3D grid the interaction energy is computed by determining and summing up the Lennard–Jones (ELJ), electrostatic (EEL), hydrogen-bonding (EHB), and entropic (ES) terms.

The GRID MIFs has been calibrated by using experimental data and the calibration was then validated by considering the accuracy of GRID prediction of the X-ray structures. Notably, the crystal packing was determined by free energy considerations, thus including consequently the enthalpic and entropic terms [75]. In the present work, we aim to qualitatively and quantitatively describe the hydrophobic interaction between a ligand and a target/protein using the DRY probe in a novel fashion.

The DRY probe has been designed to identify hydrophobic regions and it can be described as an inverse water probe. Indeed, while the Lennard–Jones interaction and charge terms are the same of the water probe, the hydrogen-bond energy is inverted to describe the destabilization generated by the polar part near the hydrophobic probe. Moreover, considering that the entropic contribution may be relevant in hydrophobic effect, a constant entropic term of – 0.848 kcal mol^{-1} was added to the total hydrophobic interaction energy [75].

The approach we propose here can be applied to describe the interaction between any pair of molecules/proteins A-B in a fixed relative position. After having removed B, the DRY probe is used to compute the hydrophobic fields surrounding the A molecule/protein, which is immersed in a 3D Cartesian grid (considering a set of equidistant points along the axis x, y and z), as schematized in Fig. 2.

The final result of the GRID calculation [51] for the A molecule/protein is thus a set of points each one

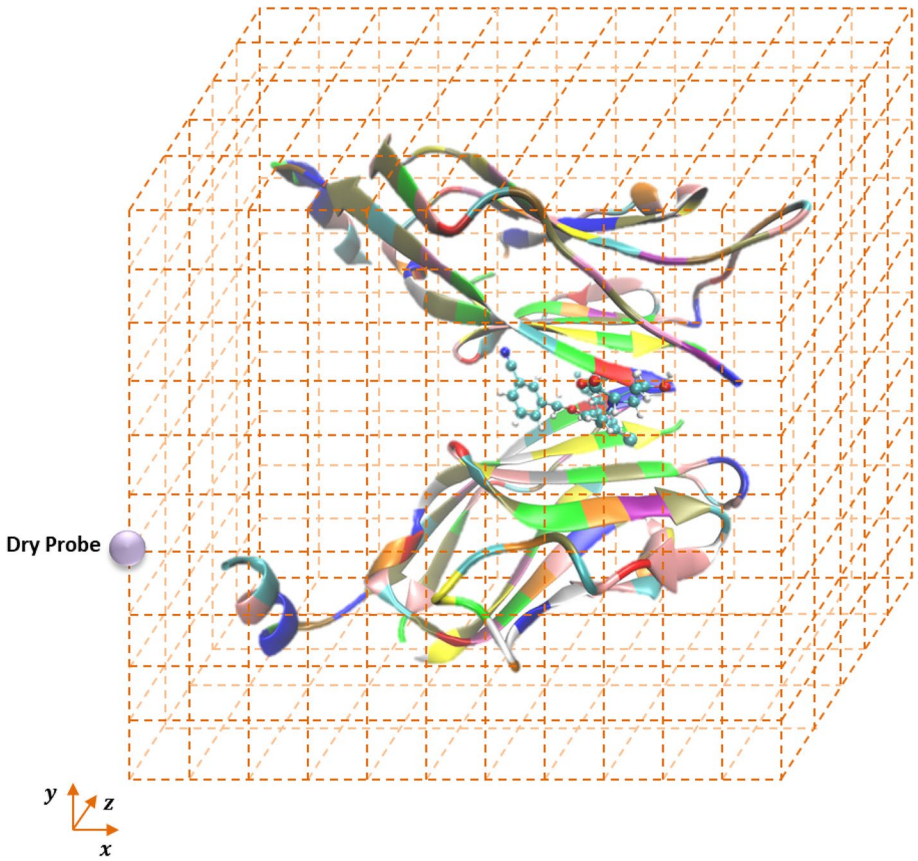

Fig. 2 Representation of 3D Cartesian grid, surrounding the A molecule/protein. The hydrophobic field is calculated by placing the DRY probe at each point of the grid (in orange)

computationally characterized by a "tuple" of values: a set of Cartesian coordinates and an interaction energy value (collectively called MIF_A).

If a MIF_A point is enclosed in a sphere centered on an atom of B it is then assigned to that atom, so that every atom in B has a set of hydrophobic energy (HE) values, HE_B*i*.

The number of points and the sum of all interaction energy values within HE_B*i* represent a reasonable measure of the hydrophobic interaction between A and the *i*-th atom of B.

Whenever a single MIF point is associated to more than one atom, it is included in the set pertaining to the nearest B atom.

In addition to the described procedure, using an in-house modified version of the GRID code, we can assign each energetic contribution MIF_A to specific A atoms.

This means that, for each interaction energy value of HE_B*i* we can identify which atoms in A contribute to the hydrophobic interaction. The entire procedure, except the GRID program, has been implemented using the Python programming language [76].

We report below the specific case of the hydrophobic interaction computed for $_{A}$PD-L1 and ligand **1** (PDB code 6R3K) as an example.

In Fig. 3 the interaction field, MIF_A, of the PD-L1 subunit A (PDB code 6R3K) together with the ligand **1**, is reported. In the figure, all the MIF_A points with an interaction less than or equal to − 1.0 kcal mol^{-1} are represented as dots surrounding each B atom.

Table 1 reports the *i* value of the ligand atom, the number of MIF_A points within each HE_B*i* set and the total value of the hydrophobic interaction energy. In the same table, we also report the list of residues which mostly contribute to the hydrophobic interaction. It is worth noting that, by this approach, we can identify all the fundamental residues [30] contributing to the hydrophobic interaction with the ligand.

We have applied the present GRID-DRY approach to investigate the hydrophobic interaction characterizing the PD-1/PD-L1 and PD-L1/BMS-ligand complexes. In the case of PD-1/PD-L1 complex we calculated the hydrophobic MIF_PD-L1, and thus the HE values of each PD-1 atom interacting with it. Then all the atomic HE_PD-1 values were grouped based on the corresponding PD-1 residues in order to compute the HE per residue. Moreover, based on the number of MIF_PD-L1 points enclosed in van der Waals radii of PD-1 atoms, we computed the energetic contribution of each PD-L1 or PD-1 residue to the corresponding hydrophobic MIF. The same approach has been used to investigate the hydrophobic interactions within PD-L1/BMS-ligands.

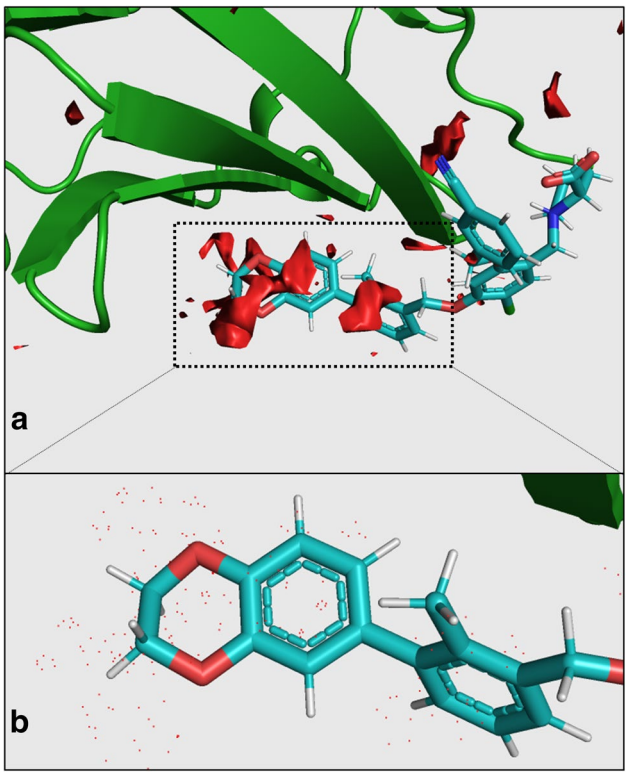

Fig. 3 **a** The interaction field (i.e. MIF_A) of the PD-L1 subunit A of PDB structure 6R3K together with ligand **1**. **b** Only the points with a MIF_A interaction strength less than or equal to − 1.0 kcal mol^{-1} are represented

Results

FMO calculations on the PD-1/PD-L1 complex

The FMO method is a valid tool to investigate PPI or protein stability. In this work, as a preliminary step, FMO calculations were performed on the heterodimer PD-1/PD-L1 in order to detect the most important residues involved in PPI. This is a crucial step to address rational drug design studies of anti-PD-L1 small molecules [53]. As shown in Fig. 4, Holak and co-workers detected three main hot regions on PD-L1: the first one (here referred to as P1) is composed by Tyr56, Glu58, Arg113, Met115 and Tyr123. The second hydrophobic pocket, P2, is composed by Met115, Ala121 and Tyr123. The last hot region is an extended groove, G, delimited by Asp26, Asp122, Tyr123, Lys124 and Arg125 [53].

All PD-L1 residues with PIE lower than or equal to − 3.0 kcal mol^{-1} as well as higher than or equal to + 3 kcal mol^{-1} were reported in Table S1 and most of the reported values are related to protein–protein interface residues.

On the other hand, the total PIE values between each PD-L1 residue and the whole PD-1 protein are summarized

Table 1 Output of GRID-DRY calculation over $_{A}$PD-L1/ligand **1** complex

Atom index	Number of MIF_A points in HE_B*i*	Interaction energy kcal mol^{-1}	Residues contributing to the total hydrophobic interaction[a]
70	1	− 1.35	Tyr56 (60.7%), Met115 (39.3%)
7	1	− 1.49	Ala121 (79.9%), Asp122 (17.9%), Tyr123 (2.2%)
32	2	− 3.15	Ile54 (73.8%), Tyr56 (1.1%), Ser117 (25.1%)
71	1	− 2.16	Tyr56 (88.2%), Met115 (11.8%)
68	2	− 2.58	Ile54 (48.7%), Tyr56 (40.9%), Gln66 (1.6%), Val68 (8.8%)
66	1	− 1.43	Ile54 (0.8%), Met115 (34.5%), Ile116 (20.8%), Ser117 (33.7%), Ala121 (10.1%)
31	1	− 1.83	Tyr56 (60.3%), Met115 (39.7%)
30	1	− 1.32	Ile54 (8.3%), Tyr56 (91.7%)
69	2	− 3.18	Ile54 (2.9%), Tyr56 (72.6%), Gln66 (17.7%), Val68 (6.9%)
36	1	− 1.01	Ala121 (91.6%), Asp122 (8.4%)
11	1	− 1.06	Ala121 (88.4%), Asp122 (9.4%), Tyr123 (2.2%)
59	1	− 1.32	Met115 (35.3%), Tyr123 (64.7%)
61	1	− 1.71	Met115 (82.0%), Tyr123 (18.0%)

[a]PD-L1 subunit A

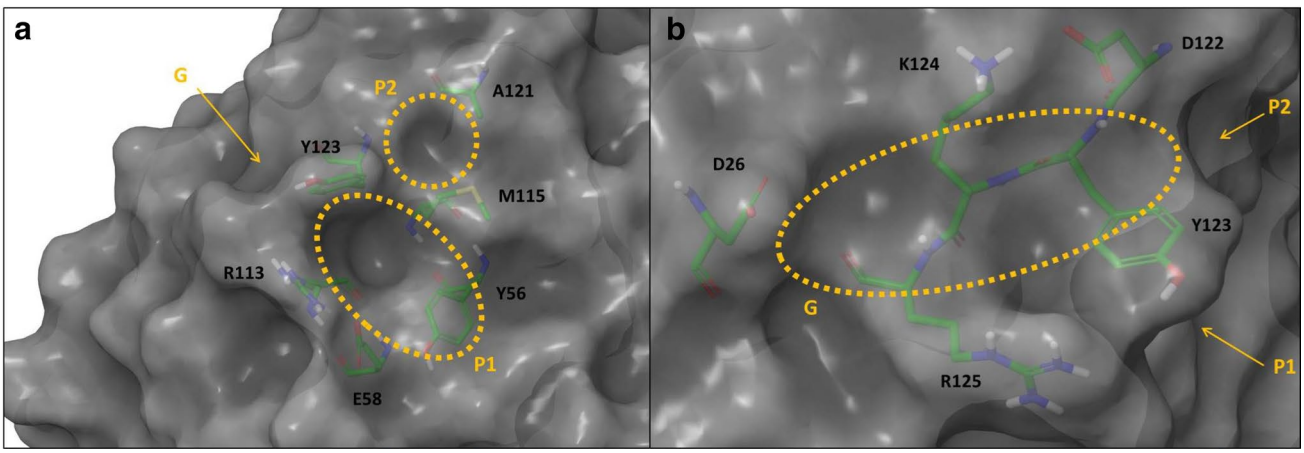

Fig. 4 The main hot regions detected on PD-L1 surface. **a** Two hydrophobic pockets were detected by Holak and co-workers [53], here indicated as P1 and P2. P1 is a region delimitated by five amino acids: Tyr56, Glu58, Arg113, Met115 and Tyr123. In adjacent position, a second reduced hydrophobic pocket, P2, is defined by Met115, Ala121 and Tyr123. **b** An extended groove, here indicated as G, was detected on specific PD-L1 region, exposed to the solvent. As a consequence, the G region is basically defined by charged residues as Asp26, Asp122, Tyr123, Lys124, Arg125

in Fig. 5 and Table 2. The chart reported in Fig. 5 is a useful representation of the PIE values; indeed, it highlights the most relevant PPIs, both attractive and repulsive. The most important attractive interactions are related to the following PD-L1 residues: Thr20 (− 34.8 kcal mol^{-1}), Asp26 (− 42.1 kcal mol^{-1}), Asp122 (− 102.7 kcal mol^{-1}), Tyr123 (− 29.5 kcal mol^{-1}), Lys124 (− 36.0 kcal mol^{-1}) and Arg125 (− 73.0 kcal mol^{-1}). Other significant interactions involve Glu58 (− 15.2 kcal mol^{-1}), Gln66 (− 13.7 kcal mol^{-1}), Glu72 (− 12.1 kcal mol^{-1}) and Arg113 (− 20.4 kcal mol^{-1}).

Interestingly, the sum of attractive PIEs computed for residues in G region (− 283.2 kcal mol^{-1}) covers 58% of the total attractive PD-1/PD-L1 interaction energy (− 490.3 kcal mol^{-1}). The PIE relative to P1 and P2 residues amounts instead only to 14% (− 68.3 kcal mol^{-1}) and to 7% (− 35.0 kcal mol^{-1}) of the total attractive interactions, respectively. The residues at regions P1, P2 and G, together, cover about 68% (− 324.4 kcal mol^{-1}) of the attractive interactions (Table 2). This is substantial evidence that the residues belonging to the G region are crucial for the PD-1/PD-L1 binding.

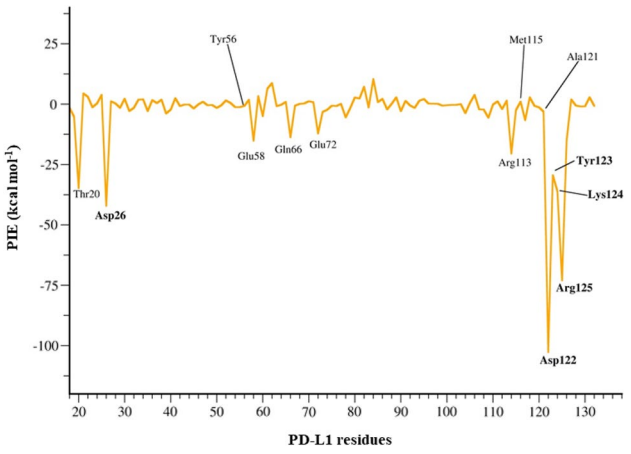

Fig. 5 PIE values of PD-L1 residues versus PD-1 protein. FMO results indicate that the most significant attractive interactions are found for residues in the G region, as Asp26, Asp122, Ty123, Lys124 and Arg125 (in bold)

PIEs, calculated between each PD-1 residue and PD-L1 protein, are shown in Table S2 in SI. The analysis of the electrostatic charge of the residues involved in the most significant attractive and repulsive interactions indicates that the attractive interactions are mainly mediated by strong electrostatic interactions between residues of PD-L1 and PD-1. In particular, the most significant pairs between the two proteins are Glu136–$_{L}$Tyr123 (− 28.9 kcal mol^{-1}), Lys78–$_{L}$Asp122 (− 94.1 kcal mol^{-1}), Asp77–$_{L}$Lys124 (− 73.5 kcal mol^{-1}), Glu136–$_{L}$Arg125 (− 90.4 kcal mol^{-1}), Gln75–$_{L}$Glu26 (− 24.8 kcal mol^{-1}). All these interactions are located in the G region, as shown in Fig. 4.

Ala-scan calculations were also performed and the results are reported in Table S3. Although with some differences—considering that the FMO method, like all ab initio approaches, cannot properly evaluate hydrophobic interactions—the Ala-scan calculations highlight the role played by most of the residues detected through the FMO method. According to the Ala-scan results, $_{L}$Tyr56, $_{L}$Glu58 and $_{L}$Tyr123 are the most relevant PD-L1 residues with ΔΔG equal to + 6.0, + 4.4 and + 3.9 kcal mol^{-1}, respectively, which were also found (although not within the same ranking) in the FMO analysis. All the five residues of the G region are listed in Table S3, again as in the FMO analysis, confirming their key role in the PD-1/PD-L1 binding.

FMO calculations on the complexes between PD-L1 and small molecules

The FMO method was also used to investigate the interaction between PD-L1 protein and all the ligands shown in Fig. 1. The first set of calculations was performed by considering the ligand as a whole in order to evaluate the total PIE, between the ligand and PD-L1 protein, and comparing them with experimental pIC$_{50}$. It is worth noting that the PIE by itself cannot be considered as the binding energy but rather provides an estimation of the strength of the ligand–protein interaction, frozen in a specific conformation [77]. However, Fedorov and co-workers have explained in great details how to perform very accurate binding energy calculations by the FMO/PCM method taking into account the deformation energies and the desolvation penalty [78].

Nevertheless, as shown in Table 3 and Fig. 6, an almost perfect linear correlation was found between the ligands PIE and the experimental pIC$_{50}$, with a computed R^2 of 0.96. This suggests that our FMO results can properly describe the ligand–protein interaction in the PD-L1/BMS-ligand system.

Table 3 also shows the PIE between the considered ligands and each subunit of PD-L1 (A and B). With the exception of the less active compounds, **6** and **5** (PDB codes 5J8O and 5N2F), the total interaction energy is more negative for subunit A than B, suggesting that ligands **1**, **2**, **3** and **4** can more strongly interact with subunit A. This evidence is particular significant for ligands **1** and **2**.

The PIE graphs for all ligands were then compared with the interaction profile computed for PD-L1 residues versus PD-1, as shown in Fig. S1, to evaluate whether the most relevant hot spots detected for PD-1/PD-L1 were also targeted

Table 3 The total PIE (kcal mol^{-1}) computed for each PD-L1/BMS-ligand complex and the corresponding experimental pIC$_{50}$ (M)

Ligand	PIE—sub A[a]	PIE—sub B[a]	Total PIE	pIC$_{50}$
1	− 124.4	− 52.6	− 177.0	8.85
2	− 127.3	− 43.1	− 170.8	8.60
3	− 78.8	− 61.8	− 140.6	7.74
4	− 57.0	− 51.3	− 108.3	7.28
5	− 58.3	− 61.2	− 119.5	7.10
6	− 31.2	− 68.0	− 99.2	6.84

[a]The total PIE of each ligand has been split in two energy contributions pertaining to subunit A and B

Table 2 The most important hot regions detected on the PD-L1 surface, their attractive PIE values and the corresponding residues

Hot-spots	Hot regions	PIE (kcal mol^{-1})	(P1 + P2 + G) PIE (kcal mol^{-1})
Tyr56, Glu58, Arg113, Met115, Tyr123	P1	− 68.3 (14%)	− 324.4 (68%)
Met115, Ala121, Tyr123	P2	− 35.0 (7%)	
Asp26, Asp122, Tyr123, Lys124, Arg125	G	− 283.2 (58%)	

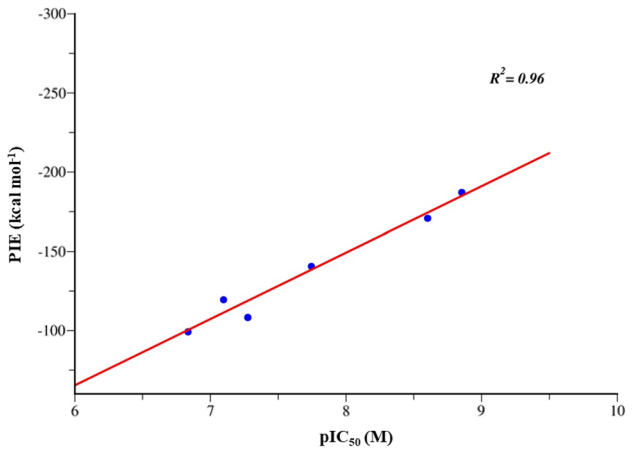

Fig. 6 Correlation between BMS-ligands total PIE and pIC_{50}. The correlation value ($R^2 = 0.96$) suggests that FMO method can correctly predict the stability of PD-L1/ligands complexes

by BMS-ligands. Interestingly, the most attractive and repulsive interaction values computed for ligands **1**–**6** follow the trend observed for PD-1/PD-L1 system, suggesting that BMS-ligands investigated here interact with most significant PD-L1 residues involved in PPI with PD-1 (see Fig. S2).

We also computed PIE values considering the fragmented ligands. The analysis of PIE graphs related to each $\mathbf{L_n}$ provides the magnitude of the interaction of each ligand portion with PD-L1 subunits A and B.

FMO calculations detect very similar interactions between $\mathbf{L_a}$ and subunits A and B, with more negative values for subunit A, as shown in Fig. S2. For each ligand, the PIE graph is a flat line indicating that no significant interactions were established by $\mathbf{L_a}$ and PD-L1. However, some common interactions were detected for ligand binding motifs; one of them is the interaction between fragment **a** and Tyr56 of both subunits A and B, with an average PIE value of -5.6 kcal mol^{-1} but the classical hydrophobic effect (not evaluable by FMO calculations) could increase the real contribution of this specific residue (Ala-scan calculations identified Tyr56 as one of the most important residues for PD-1/PD-L1 interaction). The transformation of one of the benzene ring in 2,3-dihydro-1,4-benzodiossin-6-yl moiety does not significantly improve the interaction energy with $_A$Tyr56 and $_B$Tyr56 although it increments the interactions with $_A$Gln66 and $_B$Asp122.

A similar trend was observed for the PIE computed for fragment $\mathbf{L_b}$, as reported in Fig. S3. Repulsive contacts are predicted between subunit A and ligands **1**, **2** and **6**, basically due to repulsive interactions with $_A$Asp122. For all ligands, the total interaction energy computed over subunit B, is often more negative than the corresponding values found for subunit A. The presence of halogen or other substituents on the aromatic ring does not strongly affect the PIE with $_B$Tyr56, with the exception of the CH_3O- moiety on ligand **4** (PDB code 5N2D), where a H bond is established.

FMO calculations reveal that the most attractive interactions related to $\mathbf{L_c}$ are larger for subunit A than B, with an inversion for ligand **6**. Moreover, the entity of PIE computed for $\mathbf{L_c}$ over subunit A are significantly higher than the other interaction energies detected for other ligand fragments ($\mathbf{L_a}$, $\mathbf{L_b}$), especially for the most active compounds, suggesting a possible crucial role of $\mathbf{L_c}$ in the interaction with subunit A. These results are summarized in Fig. 7. Interestingly, the PIE graph computed for ligands **4** and **3** qualitatively reproduces the interactions obtained for the PD-1/PD-L1 system. The most repulsive term has been obtained for the interaction with $_A$Arg125 and, although with less intensity, it was detected also for $_B$Arg125, located in the opposite side of $\mathbf{L_c}$.

The PIE graphs obtained for **1** and **2** (Fig. 7), the most active compounds, are characterized by an almost flat trend with strong attractive bands due to interactions with $_A$Asp122, $_A$Lys124 and $_A$Arg125, in the G region, as observed for PD-1/PD-L1. For ligand **1** the interaction with $_A$Thr20 is also significant.

Finally, the PIE values, related to $\mathbf{L_d}$ fragments (only ligands **1** and **2**), and the corresponding graphs are reported in Fig. 8. The only significant interactions are established with residues in G and specifically with $_A$Asp122 and $_A$Arg125. With the exception of such region, the energetic profiles show a flat trend. Thus, the interaction established by phenylnitrile group is crucial for the interaction with $_A$Arg125 otherwise not reached by $\mathbf{L_c}$ fragments. Considering the PIE graph obtained as a summation of interaction energies computed for $\mathbf{L_c}$ and $\mathbf{L_d}$ (see Fig. S1), ligands **1** and **2** reproduce a trend very similar to PD-L1 chart, especially for the interactions with the G region residues.

The analysis of single energy contribution to PIE (see Eq. 1) was performed by PIEDA and complete results are shown in Figs. S4–S7. Dispersion energy, E_{disp}, is shown to be a significant term in the total PIE, both for $\mathbf{L_a}$ and $\mathbf{L_b}$ moieties. It presents non zero values only for a very small number of residues, with a PIE of few kcal mol^{-1}. Considering that most of these residues are not involved in ionic or H-bond interactions, the negative values computed for E_{disp} may suggest that hydrophobic interactions play an important role (see following paragraph for extra details).

On the other hand, the PIEDA of $\mathbf{L_c}$ indicates that the main energy term is due to the electrostatic interaction, E_{es}, as shown in Fig. S6. This evidence suggests that the electrostatic interactions are crucial for a strong interaction between PD-L1 and BMS-ligands.

GRID-DRY analysis

As already mentioned, most ab initio methods cannot properly compute hydrophobic interactions which play

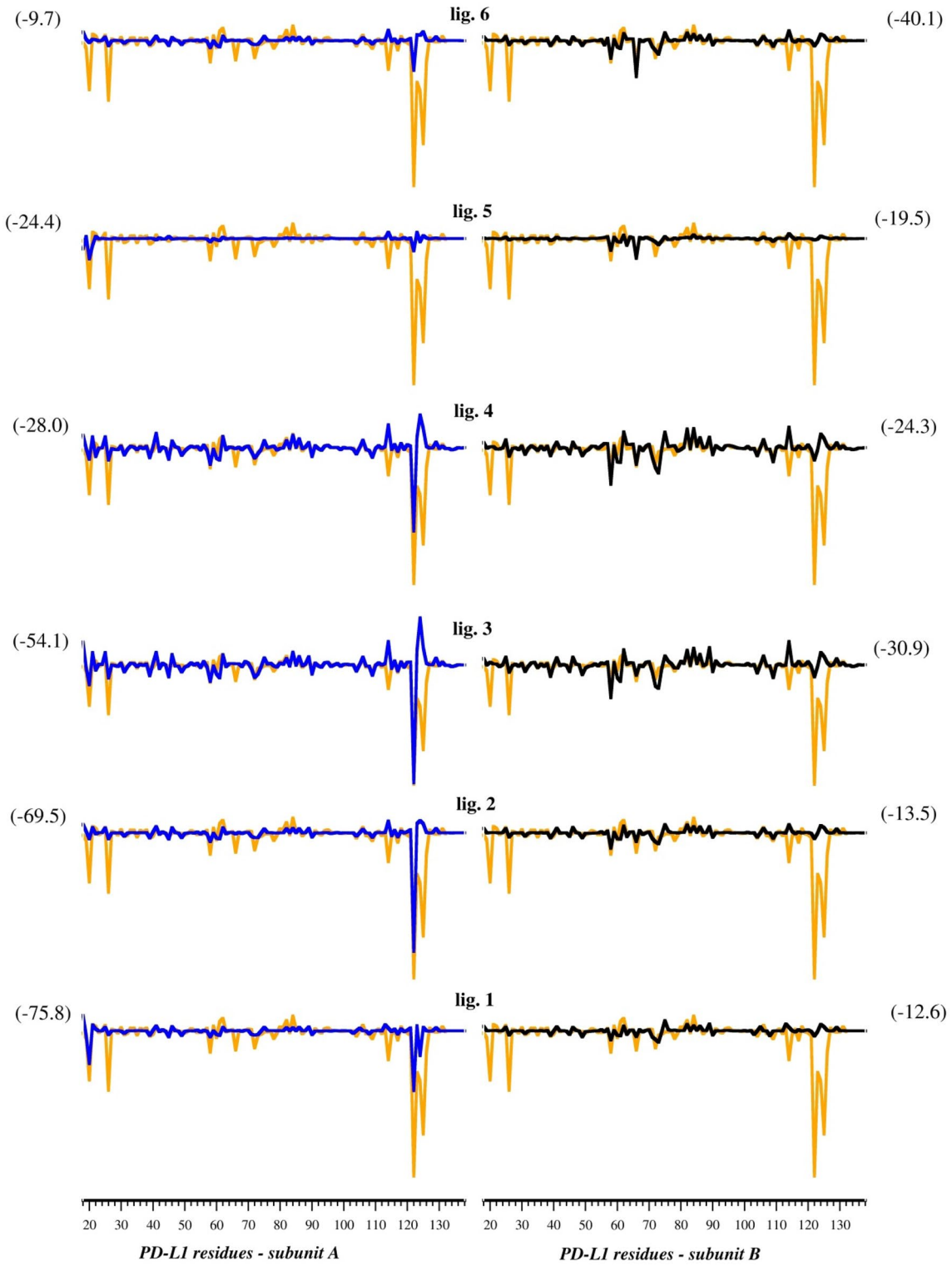

Fig. 7 PIE graph of interactions between ligands **1**–**6** L_c fragment (PDB code: 6R3K, 5NIU, 5N2D, 5N2F and 5J8O) and PD-L1 residues; the PIE values have been reported for subunits A and B in blue and in black, respectively, and their total PIEs in kcal mol^{-1} are given, on the right and on the left, respectively. The PIE graph of PD-1/PD-L1 complex is reported in orange for comparison

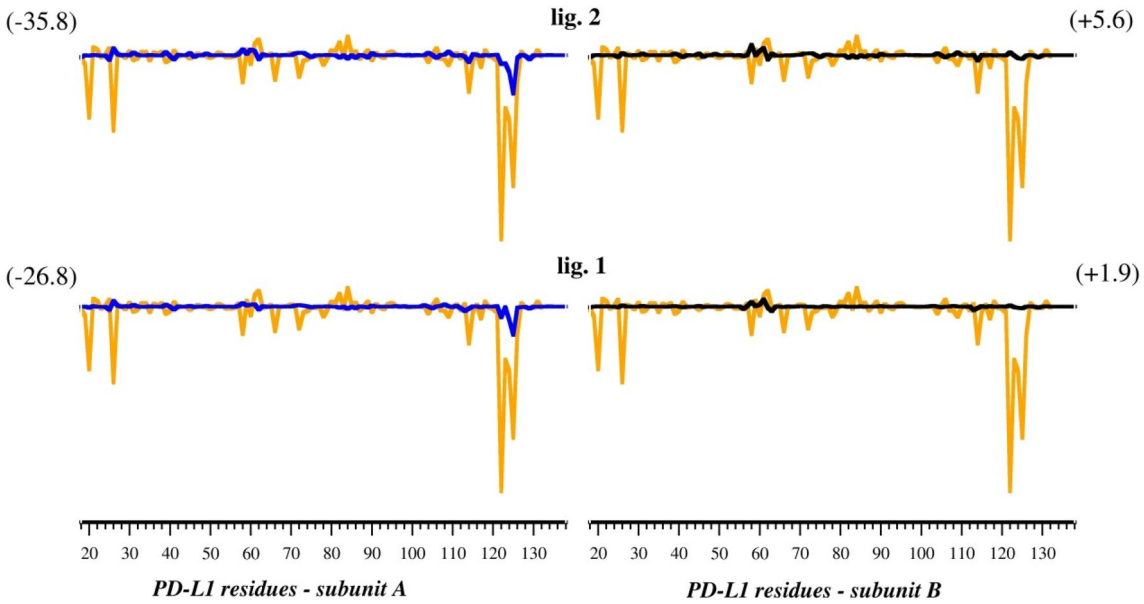

Fig. 8 PIE graph of interactions between ligands **1** and **2** $\mathbf{L_d}$ fragment (PDB code: 6R3K and 5NIU) and PD-L1 residues; the PIE values have been reported for subunits A and B in blue and in black, respectively, and their total PIEs in kcal mol^{-1} are given, on the right and on the left, respectively. The PIE graph of PD-1/PD-L1 complex is reported in orange for comparison

a significant role in the case of PPI. Indeed, some of the most important residues for PPI detected by Ala-scan are typically involved in hydrophobic interactions, like $_{L}$Tyr56, $_{L}$Tyr123 and $_{L}$Met115 for which FMO calculations assign small attractive PIE values. Instead, GRID-DRY approach was able to clearly detect those residues as crucial for hydrophobic interactions. Thus, our new GRID-DRY approach provides important complementary information about the hydrophobic contacts involved in PPIs as well as in ligand–protein interactions, significantly enhancing the accuracy of ab initio FMO prediction, with very low computational cost.

The specific results of GRID hydrophobic calculations are reported in the SI (Tables S4-S21).

For the PD-1/PD-L1 system, GRID calculations show that the energy contribution to the hydrophobic interaction of PD-L1 can mainly be ascribed to $_{L}$Ile54 (9%), $_{L}$Tyr56 (22%), $_{L}$Met115 (34%), Ala121 (7%) and $_{L}$Tyr123 (20%). In terms of hydrophobic interaction energy the most important residues are $_{L}$Val76 (− 2.4 kcal mol^{-1}), $_{L}$Met115 (− 9.6 kcal mol^{-1}), $_{L}$Ala121 (− 4.2 kcal mol^{-1}) and $_{L}$Tyr123 (− 6.4 kcal mol^{-1}). It is worth noting that ab initio FMO calculations computed very low PIE values for $_{L}$Met115 (less than − 3.0 kcal mol^{-1}) and $_{L}$Ala121 (− 3.1 kcal mol^{-1}). Indeed, Lim et al. applying the FMO method to PD-1/PD-L1 detected only two hot regions, P1 and G, because the calculated PIE values of the hydrophobic residues $_{L}$M115 and $_{L}$A121 (P2 region) resulted to be not significant [50]. Thus, the GRID-DRY method demonstrates to be essential to correctly assess the importance of those residues in PPI process.

PD-1 residues involved in hydrophobic contacts are instead: Ile126, Leu128, Ala132 and Ile134 with a total HE of − 16.1, − 4.0, − 17.6 and − 11.9 kcal mol^{-1}, respectively. The total hydrophobic energy is − 49.6 and − 26.8 kcal mol^{-1} for HE_PD-1 and HE_PD-L1, respectively (Table S5 and S7). These results suggest that PD-L1 protein–protein interface is characterized by a larger hydrophobic component than PD-1 protein.

The hydrophobic MIF_PD-L1, associated to subunits A and B, were also evaluated for each ligand–protein complex. In Fig. 9 we report the average energy contribution to the hydrophobic field by PD-L1 residues interacting with ligands **1**–**6**.

As for the electrostatic interaction, the most significant PD-L1 residues involved in hydrophobic interactions are the same involved in PD-1/PD-L1 interaction, that is: $_{A}$Tyr56, $_{A}$Met115, $_{A}$Ala121 and $_{A}$Tyr123 of subunit A. Residues of subunit B showed a similar trend but about 40% of all hydrophobic contacts is attributed to $_{B}$Tyr56, suggesting the great importance of such residue in this specific interaction. This analysis suggests that the hydrophobic residues of two subunits interact with the ligands with a different strength. Specifically, subunit A interacts basically via $_{A}$Tyr56, $_{A}$Met115, $_{A}$Ala121 and $_{A}$Tyr123 whereas subunit B via $_{B}$Ile54, $_{B}$Tyr56, $_{B}$Met115 and $_{B}$Ala121. The HE values, computed for each ligand with respect to subunits A and B, are shown in Table 4. Moreover, the HE values computed for each ligand all show that the hydrophobic energy for subunit B is always twice than subunit A, suggesting that the hydrophobic interaction is more important for subunit B than A.

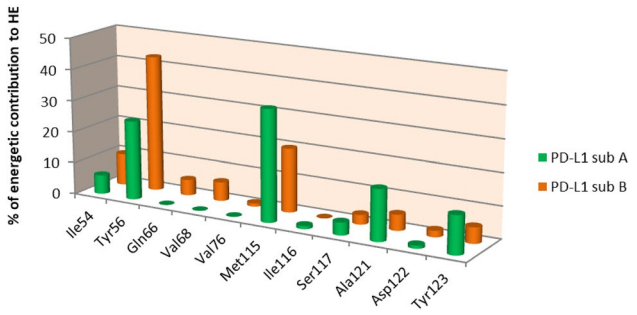

Fig. 9 Bar chart of the most significant hydrophobic contacts between ligands **1**–**6** and PD-L1, detected by the GRID-DRY approach. On the y axis the percentage average value of the contribution of each residue to HE, computed for PD-L1 subunits A and B, in green and orange, respectively

Table 4 Hydrophobic energy (HE) computed between ligands **1**–**6** and PD-L1 subunits A and B, using the GRID-DRY approach

Ligand	HE (kcal mol^{-1})		HE($_B$PD-L1)/ HE($_A$PD-L1)
	$_A$PD-L1	$_B$PD-L1	
1	− 22.524	− 43.275	1.9
2	− 22.277	− 40.328	1.8
3	− 20.033	− 41.58	2.1
4	− 18.871	− 39.221	2.1
5	− 15.587	− 38.857	2.5
6	− 14.111	− 30.058	2.1

In order to shed some light onto the hydrophobic interactions we calculated the HE of each ligand fragment, versus both subunits A and B. Very interestingly, for subunit A the HE is associated almost exclusively to $\mathbf{L_a}$ fragment. This suggests that hydrophobic contact between PD-L1 subunit A and the ligands is basically to be ascribed to the biphenyl moiety.

The substitution of the phenyl ring with 2,3-dihydro-1,4-benzodiossin-6-yl moiety does not affect uniformly the HE, considering that it boosts this type of interactions for **1** and **2** but not for **5**. An analysis of the number of points associated to subunit A hydrophobic field indicates that $\mathbf{L_a}$ of ligand **5** interacts with a smaller number of points than **1** and **2**, suggesting that the different binding pose can affect the fitting of $\mathbf{L_a}$ with $_A$PD-L1 hydrophobic field. The analysis of the contribution of $_A$PD-L1 residues reveals that both P1 and P2 regions interact with $\mathbf{L_a}$ by means of $_A$Tyr56, $_A$Met115, $_A$Ala121 and $_A$Tyr123.

On the other hand, when considering $_B$PD-L1, GRID calculations highlight attractive HE values for $\mathbf{L_a}$ and $\mathbf{L_b}$ fragments. However, more significant values were computed in most cases for $\mathbf{L_b}$ fragment, basically interacting with subunit B, by means of $_B$Tyr56 ($_B$P1 region).

Discussion

The immunologic checkpoint PD-1 and its ligand PD-L1 are important targets for new anticancer drugs [79] and a lot of effort was put to discover small-molecule drugs acting on PD-L1. This process was also boosted by the availability of the binding pose of six chemical compounds patented by Bristol–Mayers Squibb [19, 20]. They are all members of a specific class of small drugs characterized by the (2-methyl-3-biphenylyl)methanol scaffold which links to another aromatic ring. Their X-ray structures showed, for the first time, the binding region on PD-L1 in homodimer complex, $_A$PD-L1/ligand/$_B$PD-L1. Starting from them, with the aim to provide useful information for the design of new anti-PD-L1 drugs, we applied a combination of the ab initio FMO method and the GRID-DRY approach on PD-1/PD-L1 and PD-L1/BMS-ligands (**1**–**6**, Fig. 1). The investigation of PD-1/PD-L1 interaction shows that residues characterizing the PPI are $_L$Asp26, $_L$Asp122, $_L$Tyr123, $_L$Lys124 and $_L$Arg125, involved in strong electrostatic interactions, and $_L$Tyr56, $_L$Met115, $_L$Ala121 and $_L$Tyr123 involved in hydrophobic contacts. These results are in good agreement with structural analysis by Holak and co-workers and with recent computational works [52, 80, 81]. Moreover, most of these residues were found also involved in the interactions between PD-L1 and some mAbs [82].

The most important residues characterizing the electrostatic and hydrophobic interaction in PD-1/PD-L1 complex were found for all compounds investigated here, and they are particularly relevant for the most active molecules **1** and **2**.

Indeed, ligands **1** and **2**, with one negative and one positive charge in the $\mathbf{L_c}$ portion, show the most negative PIE, reproducing the electrostatic pair interactions $_L$Asp77–Lys124, $_L$Asp122–Lys78 and $_L$Tyr123–Tyr68 detected in PD-1/PD-L1, as shown in Fig. 10.

On the contrary, the positively charged ligands, **3** and **4**, establish a strong repulsive interaction with $_A$Arg125, although the contact with $_A$Asp122 is attractive. Hence, according to our FMO results, the most active compounds are characterized by the highest PIE values for G region residues ($_A$Asp122, $_A$Lys124 and $_A$Arg125), allowing us to speculate that these specific interactions can be used as a diagnostic signature to evaluate the affinity of BMS-ligands type.

Based on this, in order to build new ligands for PD-L1, the G region should be the principal hot region and therefore could be used as a starting point for receptor-based drug design process. According to this suggestion, as schematized in Fig. 11, new molecules should have both a negatively and a positively charged moiety,

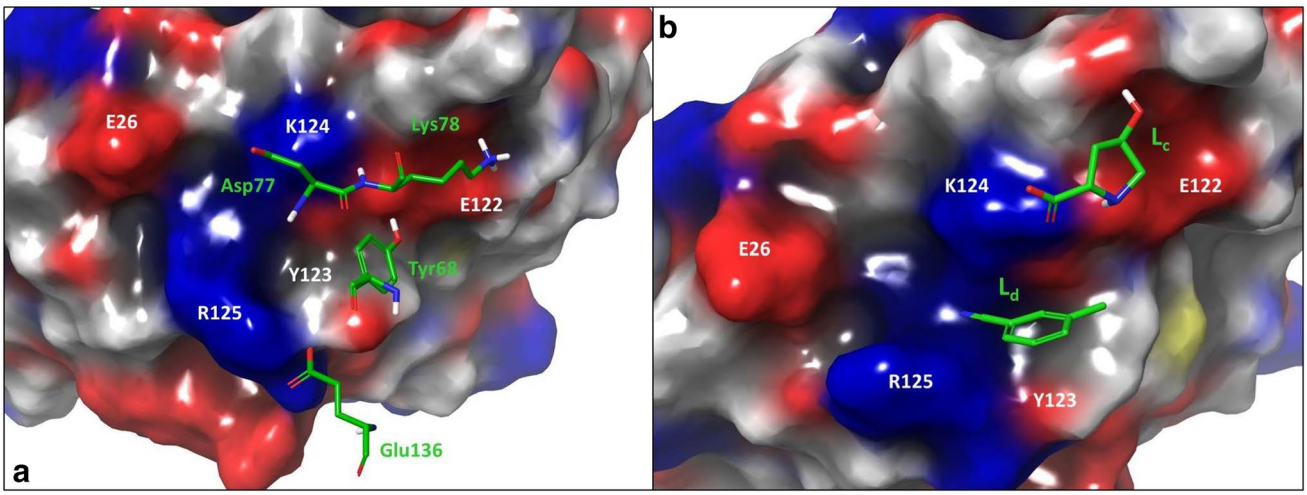

Fig. 10 **a** Charged residues (grey for neutral, blu for positively charged, red for negatively charged) on PD-L1 surface. The groove residues of PD-L1 are reported using one letter code, in white, while the most important PD-1 residues are colored in green, and indicated with a three letter code. **b** the PD-1 residues are replaced by the fragments $\mathbf{L_c}$ and $\mathbf{L_d}$ of ligand **1**. The (2R, 4R)-4-hydroxypyrrolidine-2-carboxylic acid group ($\mathbf{L_c}$) is involved in ionic interactions with with E122 and K124, as for Lys78 and Asp77. The benzonitrile moiety interacts with Y123 by means of pi-pi contact in a similar way to Tyr68, in PD-1/PD-L1 complex. The nitrile group can establish H-bond interaction with Y123, reproducing Glu136 contact

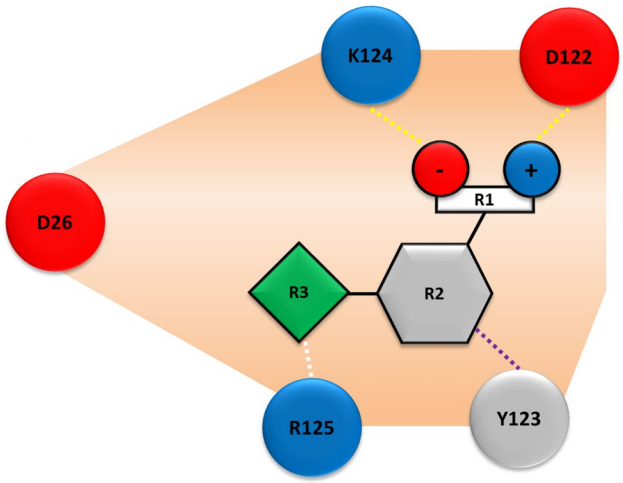

Fig. 11 Schematic representation of a possible pharmacophore targeting the G region, designed on the base of FMO results. R1 is a specific group characterized by the presence of one negatively and one positively charged groups. They must have a specific space orientation so to optimize the ionic interactions (represented by a dashed yellow line) with D122 and K124. R1 is linked to R2, an aromatic moiety, which is involved in π–π interaction (dashed purple line) with Y123. Finally, R2 may hold a H-bond acceptor group, R3, able to interact with R125 (dashed white line). R3 may be also a H-bond donor in order to establish an interaction with D26

with an appropriate spatial orientation, in order to maximize the electrostatic interaction with $_{L}$Asp122 and $_{L}$Arg125/$_{L}$Lys124, reproducing the PD-1 arrangement of residues Asp77–Lys78 (R1 in Fig. 11).

The oppositely charged groups could also be replaced by H bond acceptor and donor moieties while the presence of a single charged group destabilizes the interaction with residues located in G region. The presence of an aromatic group with a H-bond acceptor moiety, like the 3-benzonitrile substituent, on the one side reproduces the PD-1 Tyr68 action, interacting with $_{L}$Tyr123 via pi-pi contacts (R2 in Fig. 11) and, on the other, a H-bond acceptor moiety (e.g. the nitrile group) able to reach the Arg125 (R3 in Fig. 11).

While electrostatic interactions are decisive to hit the G region, hydrophobic contacts play an important role for BMS-ligands MAO, characterized by PD-L1 dimerization. GRID-DRY results indicate that PD-L1 residues $_{L}$Tyr56, $_{L}$Met115, $_{L}$Ala121 and $_{L}$Tyr123 are crucial for the hydrophobic interactions with PD-1. These residues are also involved in the hydrophobic contacts between BMS-ligands bound to homodimer PD-L1/PD-L1, where ligands are located between two proteins. A detailed analysis of these contacts reveals that the hydrophobic interaction between ligands and subunits A and B does not present the same magnitude. Indeed, the hydrophobic energy calculated for subunit B is always twice that for subunit A.

Specifically, while the hydrophobic interaction between $_{A}$PD-L1 and BMS-ligands can be almost totally ascribed to the biphenyl group ($\mathbf{L_a}$) with P1 and P2, subunit B interacts basically via the $_{B}$Tyr56 residue with the second aromatic system ($\mathbf{L_b}$) and only partially with the $\mathbf{L_a}$ fragment. Thus, $_{B}$Tyr56 acts as a crucial contact point between ligands and subunit B. These results can also explain why the aromatic rings system (the biphenyl group linked to another aromatic

ring) is the smallest fragment in BMS-ligands with the PD-L1 binding ability [21]. Indeed, it is the smallest structure with chemical-geometric features able to hit P1 and P2 of subunit A and $_{B}$Tyr56 (P1 region), thus acting as hydrophobic glue between the two PD-L1 units. Thus, since the electrostatic interactions computed by FMO are less important for $_{B}$PD-L1/ligand we can suppose that the hydrophobic interaction is the driving force that connects the ligand to a second PD-L1 unit. This point may be relevant to design new drugs acting on single PD-L1 protein.

All these evidences, detected for each ligand investigated here, allow us to envisage a possible MOA of the BMS-ligands characterized by biphenyl moiety. The $\mathbf{L_c}$ and $\mathbf{L_d}$ portions of ligands, characterized by the presence of charged groups (e.g. the (2R, 4R)-4-hydroxypyrrolidine-2-carboxylic group for ligand **1**), are the first to recognize the target due to specific electrostatic pairing with charged residues in G, in particular with $_{A}$Asp122, $_{A}$Tyr123, $_{A}$Lys124 and $_{A}$Arg125. Then, the biphenyl moiety establishes hydrophobic contacts with $_{A}$Tyr56, $_{A}$Met115, $_{A}$Ala121 and $_{A}$Tyr123, located in regions P1 and P2. In this pose, the ligand exposes the aromatic portions as $\mathbf{L_a}$ and $\mathbf{L_b}$ fragments, which interact with Tyr56 of another PD-L1 protein. The consequent water expulsion increases the efficiency of London interactions stabilizing the complex. This hypothesis was firstly proposed by Holak and co-workers based on docking simulations of BMS-1001 and − 1166 which provided a favorable binding mode only for $_{A}$PD-L1, but not $_{B}$PD-L1 [21]. Our results, obtained with a new mixed QM/MM method, confirm this hypothesis. Recently, a new computational study based on MD calculations proposed the same MOA to justify the dimerization of PD-L1 by BMS-ligands [80].

Our outcomes concerning the most relevant residues in this interaction are in good agreement with the results of three recent studies. In particular, Ding et al. by means of alchemical free energy calculations found that the most important PD-L1 residues involved in PPI are $_{L}$Asp26, $_{L}$Ile54, $_{L}$Tyr56, $_{L}$Met115, $_{L}$Tyr123 and $_{L}$Lys124 [83]. Moreover, they found that Tyr68, Il126 and $_{L}$Tyr123 represent a hydrophobic cluster contributing significantly to the binding energy. Our GRID-DRY calculations indicate the same strong hydrophobic interactions of Ile126, otherwise not detected by the sole ab initio FMO calculations. Fesik et al. describe a fragment-based approach that allowed identifying and crystallizing fragments ligands interacting with PD-L1 [84]. The crystal structures reveal that all fragments share a similar binding pose inside the hydrophobic pocket formed by two PD-L1 units. The investigated fragments are mainly hydrophobic and interact with $_{L}$Ile54, $_{L}$Tyr56, $_{L}$Met115, $_{L}$Tyr123, and $_{L}$Ala121, all residues of P1 and P2 regions, as predicted by our GRID-DRY calculations as well. These evidences again support the hypothesis that the biphenyl moiety is crucial for homodimerization of PD-L1 unit.

Finally, Mejías and Guirola derived a putative pharmacophore for the PD-L1 inhibition through the cosolvent molecular dynamics simulation [85], characterized by seven hydrophobic features (interacting with $_{L}$M115, $_{L}$A121, $_{L}$Y123, $_{L}$I54 and $_{L}$Y56), one positive/acceptor interacting with $_{L}$E58, one negative/donor interacting with LArg125 and one polar feature. These results confirm our GRID-DRY predictions concerning hydrophobic hot spots. However, their proposed pharmacophore model could not detect ionic interactions with $_{L}$Asp122 and $_{L}$Lys124 which are instead crucial to hit G region, according to our FMO results.

Recently the FMO method has been applied by Lim et al. [50] to PD-1/PD-L1 heterodimer and to several PD-L1/ligand complexes including those of the present investigation, with the exception of BMS-1156 and BMS-1001 ligands (**1** and **2** in our work, respectively) which are the most active anti-PD-L1 small drugs with known crystal structures. However, they analyzed FMO results by using the 3-dimensional scattered pair interaction energies (3D-SPIEs) analysis tool, limiting their discussion to PD-L1 hot spots and hot regions. At variance with their approach, since our main goal consists of defining a new pharmacophore model for novel anti-PD-L1 molecules, our study starts from PD-1/PD-L1 heterodimer to focus on all PD-L1/BMS-ligands complexes in a second stage. To this aim, we applied FMO method in the specific way typical of the drug discovery process, splitting up each ligand into three/four fragments according to the ligand functional groups. This approach allowed us to study in great details how each functional group interacts with PD-L1 residues, improving the characterization of structure–activity relationship (SAR) of this class of compounds. In this way, as shown previously, we were able to collect new features of BMS-ligands binding modes especially for the most active compounds BMS-1156 and BMS-1001, and to introduce here a specific pharmacophore model of PD-L1 inhibitor.

Although the present study detected the G region as the possible crucial hot region, it does not hold the features of a typical binding pocket, with high exposure to the solvent. Nevertheless, residues composing the G region are all flexible amino acids and some open conformations are possible. Transient druggable pockets can assume an open conformation only for few instants due to conformational fluctuations and molecular dynamics can be successfully used to detect them [86, 87]. Gohlke and co-workers proposed an effective computational procedure, based on MD and molecular docking, to investigate the conformational plasticity and finding potential transient pockets [88, 89]. Such computational approaches may be applied to verify the hypothesis about the G region as a possible binding pocket for novel anti-PD-L1 small-molecule drugs.

Conclusions

We propose here a novel computational approach by combining an ab initio FMO calculations and a new GRID-DRY approach in order to characterize the PD-L1 binding site and thus providing useful information to address the rational design of new anti-PDL1 small drugs. The FMO method allows us to investigate the interactions with ab initio accuracy while GRID-DRY approach is a computational fast tool to evaluate the most important hydrophobic contacts. To the best of our knowledge this is the first work where the combination of GRID method with FMO approach has been proposed in order to fill the lack of ab initio methods concerning the calculation of hydrophobic contribution. Their combination is shown here to be a powerful and versatile tool to study protein–protein as well as protein-ligands interaction.

In agreement with previous computational results, we found $_{A}$Asp122, $_{A}$Tyr123, $_{A}$Lys124 and $_{A}$Arg125 as the most important residues for electrostatic interactions between ligands and PD-L1 subunit A. All these residues are located in a precise PD-L1 region (here called G region), suggesting their crucial role for the PPI of PD-1/PD-L1 as well as for PD-L1/BMS-ligands binding. In particular BMS-ligands bind more strongly subunit A than B, especially when they are characterized by the presence of two oppositely charged groups targeting the G region, with specific space orientation.

On the other hand, we found that the hydrophobic contacts characterizing PD-L1/BMS-ligand interactions play a crucial role in the formation of homodimer PD-L1/BMS-ligand/PD-L1 complex. The most important involved residues are $_{A}$Tyr56, $_{A}$Met115, $_{A}$Ala121, $_{A}$Tyr123 and $_{B}$Ile54, $_{B}$Tyr56, $_{B}$Met115 and $_{B}$Ala121 for subunit B. All these residues establish hydrophobic interaction with 4-phenylbenzyloxy- group, shared by all BMS-ligands, acting as "hydrophobic glue" promoting PD-L1 dimerization.

In conclusion, we suggest that G region, delimited by Asp26, Asp122, Tyr123, Lys124 and Arg125, is very relevant in PD-L1 PPI and the search for novel chemical entities specifically able to target these residues may lead to the discovery of new anti-PD-L1 small molecules. Further computational investigations, such as MD and receptor-based drug design studies, are necessary to assess this hypothesis and the druggability of G region.

Supporting information

Further results of FMO calculations and GRID-DRY analysis for PD-1/PD-L1 complex as well as for each PD-L1/BMS-ligand are available free of charge in Supporting_Information.pdf.

Acknowledgement We thank the Ministry of Education, University and Research (MIUR) for financial support. Moreover, we are thankful to Prof. Alessandro Marrone for his suggestions and useful discussions.

Author Contributions The manuscript was written through contributions of all authors. All authors have given approval to the final version of the manuscript.

Compliance with ethical standards

Conflict of interest The authors declare no competing financial interest.

References

1. Pardoll DM (2012) The blockade of immune checkpoints in cancer immunotherapy. Nat Rev Cancer 12:252–264
2. Mahoney KM, Freeman GJ, McDermott DF (2015) The next immune-checkpoint inhibitors: PD-1/PD-L1 blockade in melanoma, PD-1/PD-L1 inhibitors. Clin Ther 37(4):764–782
3. Blank C, Gajewski TF, Mackensen A (2005) Interaction of PD-L1 on tumor cells with PD-1 on tumor-specific T cells as a mechanism of immune evasion: implications for tumor immunotherapy. Cancer Immunol Immunother 54:307–314
4. Wilkinson E (2015) Nivolumab success in untreated metastatic melanoma. Lancet Oncol 16:e9
5. Bagcchi S (2014) Pembrolizumab for treatment of refractory melanoma. Lancet Oncol 15:e419
6. Lipson EJ, Forde PM, Hammers H, Emens LA, Taube JM, Topolian SL (2015) Antagonists of PD-1 and PD-L1 in cancer treatment. Semin Oncol 42:587–600
7. Iwai Y, Ishida M, Tanaka Y, Okazaki T, Honjo T, Minato N (2002) Involvement of PD-L1 on tumor cells in the escape from host immune system and tumor immunotherapy by PD-L1 blockade. Proc Natl Acad Sci USA 99:12293–12297
8. Herbst RS, Soria JC, Kowanetz M, Fine GD, Hamid O, Gordon MS, Sosman JA, McDermott DF, Powderly JD, Gettinger SN, Kohrt HE, Horn L, Lawrence DP, Rost S, Leabman M, Xiao Y, Mokatrin A, Koeppen H, Hegde PS, Mellman I, Chen DS, Hodi FS (2014) Predictive correlates of response to the anti-PD-L1 antibody MPDL3280A in cancer patients. Nature 515:563–567
9. Brahmer JR, Tykodi SS, Chow LQM, Hwu W, Topalian SL, Hwu P, Drake CG, Camacho LH, Kauh J, Odunsi K, Pitot CH, Hamid O, Bhatia S, Martins R, Eaton K, Chen S, Salay TM, Alaparthy S, Grosso JF, Korman AJ, Parker SM, Agrawal S, Goldberg SM, Pardoll DM, Gupta A, Wigginton JM (2012) Safety and activity of anti-PD-L1 antibody in patients with advanced cancer. N Engl J Med 366:2455–2465
10. Philips GK, Atkins M (2015) Therapeutic uses of anti-PD-1 and anti-PD-L1 antibodies. Int Immunol 27:39–46
11. Naidoo J, Page DB, Li BT, Connell LC, Schindler K, Lacouture ME, Postow MA, Wolchok JD (2015) Toxicities of the

anti-PD-1 and anti-PD-L1 immune checkpoint antibodies. Ann Oncol 26:2375–2391
12. Chen T, Li Q, Liu Z, Chen Y, Feng F, Sun H (2019) Peptide based and small synthetic molecule inhibitors on PD/PD-L1 pathway: a new choice for immunotherapy? Eur J Med Chem 161:378–398
13. Zhan M, Hu X, Liu X, Ruan B, Xu J, Liao C (2016) From monoclonal antibodies to small molecules: the development of inhibitors targeting the PD-1/PD-L1 pathway. Drug Discovery Today 21(6):1027–1036
14. Ribas A, Wolchok JD (2018) Cancer immunotherapy using checkpoint blockade. Science 359:1350–1355
15. Chowdhury PS, Chamoto K, Honjo T (2018) Combination therapy strategies for improving PD-1 blockade efficacy: a new era in cancer immunotherapy. J Intern Med 283:110–120
16. Chupak LS, Zheng X (2015) Compounds useful as immunomodulators. WO2015034820A1
17. Chupak LS, Ding M, Martin SW, Zheng X, Hewawasam P, Connolly TP, Xu N, Yeung K-S, Zhu J, Langley DR, Tenney DJ, Scola PM, Mingo PA (2015) Compounds useful as immunomodulators. WO2015160641
18. Abdel-Magid AF (2015) Inhibitors of the PD-1/PD-L1 pathway can mobilize the immune system: an innovative potential therapy for cancer and chronic infections. ACS Med Chem Lett 6:489–490
19. Zak KM, Grudnik P, Guzik K, Zieba BJ, Musielak B, Dömling A, Dubin G, Holak TA (2016) Structural basis for small molecule targeting of the programmed death ligand 1 (PD-L1). Oncotarget 7:30323–30335
20. Guzik K, Zak KM, Grudnik P, Magiera K, Musielak B, Törner R, Skalniak L, Dömling A, Dubin G, Holak TA (2017) Small-molecule inhibitors of the programmed cell death-1/programmed death-ligand 1 (PD-1/PD-L1) interaction via transiently induced protein states and dimerization of PD-L1. J Med Chem 60(77):5857–5867
21. Skalniak L, Zak KM, Guzik K, Magiera K, Musielak B, Pachota M, Szelazek B, Kocik J, Grudnik P, Tomala M, Krzanik S, Pyrc K, Dömling A, Dubin G, Holak T (2017) A small-molecule inhibitors of PD-1/PD-L1 immune checkpoint alleviate the PD-L1-induced exhaustion of T-cells. Oncotarget 8:72167–72181
22. Sasikumar PGN, Ramachandra M, Naremaddepalli SSS (2015) 1,2,4-Oxadiazole derivatives as immunomodulators. US20150073024
23. Sasikumar PGN, Ramachandra M, Vadlamani SK, Vemula KR, Satyam LK, Subbarao K, Shrimali RK, Kandepu S (2013) Immunosuppression modulating compounds. EP2585099A2
24. Sasikumar PGN, Ramachandra M, Naremaddepalli SSS (2013) Peptidomimetic compounds as immunomodulators. WO2013132317A8
25. Shrimali KR, Subbarao K (2012) Therapeutic compounds for immunomodulation. WO2012168944A1
26. Miller MM, Mapelli C, Allen MP, Bowsher MS, Boy KM, Gillis EP, Langley DR, Mull E, Poirier MA, Sanghvi N (2014) Macrocyclic inhibitors of the pd-1/pd-l1 and cd80(b7-1)/pd-l1 protein/protein interactions. WO2014151634A1
27. Sasikumar PGN, Ramachandra M, Naremaddepalli SSS (2015) Cyclic peptidomimetic compounds as immunomodulators. WO2015033303A1
28. Magiera-Mularz K, Skalniak L, Zak KM, Musielak B, Rudzinska-Szostak E, Berlicki Ł, Kocik J, Grudnik P, Sala D, Zarganes-Tzitzikas T, Shaabani S, Dömling A, Dubin G, Holak TA (2017) Bioactive macrocyclic inhibitors of the PD-1/PD-L1 immune checkpoint. Angew Chemie Int Ed 56:13732–13735
29. Weinmann H (2016) Cancer immunotherapy: selected targets and small-molecule modulators. ChemMedChem 11:450–466
30. Guzik K, Tomala M, Muszak D, Konieczny M, Hec A, Błaszkiewicz U, Pustuła M, Butera R, Dömling A, Holak TA (2019) Development of the inhibitors that target the PD-1/PD-L1 interaction—a brief look at progress on small molecules, peptides and macrocycles. Molecules 24:2071
31. Wells JA, McClendon CL (2007) Reaching for high-hanging fruit in drug discovery at protein–protein interfaces. Nature 450:1001–1009
32. Arkin RM, Wells JA (2004) Small-molecule inhibitors of protein–protein interactions: progressing towards the dream. Nat Rev Drug Discovery 3:301
33. Fry DC (2006) Protein–protein interactions as targets for small molecule drug discovery. Biopolymers 84:535–552
34. Bogan AA, Thorn KS (1998) Anatomy of hot spots in protein interfaces. J Mol Biol 280:1–9
35. Li J, Liu Q (2009) 'Double water exclusion': a hypothesis refining the O-ring theory for the hot spots at protein interfaces. Bioinformatics 25(6):743–750
36. Moreira IS, Fernandes PA, Ramos MJ (2007) Hot spots—a review of the protein–protein interface determinant amino-acid residues. Proteins 68:803–812
37. Kortemme T, Baker D (2002) A simple physical model for binding energy hot spots in protein–protein complexes. PNAS 99(22):14116–14121
38. Morrow JK, Zhang S (2012) Computational prediction of hot spot residues. Curr Pharm Des 18(9):1255–1265
39. Koes D, Khoury K, Huang Y, Wang W, Bista M, Popowicz GM, Wolf S, Holak TA, Dömling A, Camacho CJ (2012) Enabling large-scale design, synthesis and validation of small molecule protein-protein antagonists. PlosOne 7(3):e32839
40. Mora JS, Assi SA, Fernandez-Fuentes N (2010) Presaging critical residues in protein interfaces-web server (PCRPi-W): a web server to chart hot spots in protein interfaces. PlosOne 5(8):e12352
41. Fedorov DG, Nagata T, Kitaura K (2012) Exploring chemistry with the fragment molecular orbital method. Phys Chem Chem Phys 14:7562–7577
42. Kitaura K, Ikeo E, Asada T, Nakano T, Uebayasi M (1999) Fragment molecular orbital method: an approximate computational method for large molecules. Chem Phys Lett 313:701–706
43. Nakano T, Kaminuma T, Sato T, Akiyama Y, Uebayasi M, Kitaur K (2000) Fragment molecular orbital method: application to polypeptides. Chem Phys Lett 318:614–618
44. Nagase K, Kobayashi H, Yoshikawa E, Kurita N (2009) Ab initio molecular orbital calculations on specific interactions between urokinase-type plasminogen activator and its receptor. J Mol Graphics Modell 28:46–53
45. Paciotti R, Storchi L, Marrone A (2019) An insight of early PrP-E200K aggregation by combined molecular dynamics/fragment molecular orbital approaches. Proteins 87:51–61
46. Storchi L, Paciotti R, Re N, Marrone A (2015) Investigation of the molecular similarity in closely related protein systems: the PrP case study. Proteins 83:1751–1765
47. Fukuzawa K, Komeiji Y, Mochizuki Y, Kato A, Nakano T, Tanaka S (2006) Intra- and intermolecular interactions between cyclic-AMP receptor protein and DNA: ab initio fragment molecular orbital study. J Comput Chem 27:948–960
48. Nemoto T, Fedorov DG, Uebayasi M, Kanazawa K, Kitaura K, Komeiji Y (2005) Ab initio fragment molecular orbital (FMO) method applied to analysis of the ligand–protein interaction in a pheromone-binding protein. Comput Biol Chem 29:434–439
49. Lim HC, Chun JH, Hwang SB, Kim JW, No KT (2018) Specific interactions of protein-protein interaction between human programmed death 1 (PD-1) and its ligand 1 (PD-L1) with ab initio fragment molecular orbital method. Biophys J 114(3):423A
50. Lim H, Chun J, Jin X, Kim J, Yoon JH, No KT (2019) Investigation of protein-protein interactions and hot spot region between PD-1 and PD-L1 by fragment molecular orbital method. Sci Rep 9:16727

51. Goodford PJ (1985) A computational procedure for determining energetically favorable binding sites on biologically important macromolecules. J Med Chem 28:849–857
52. Zak KM, Kitel R, Przetocka S, Golik P, Guzik K, Musielak B, Dömling A, Dubin G, Holak TA (2015) Structure of the complex of human programmed death 1, PD-1, and its ligand PD-L1. Structure 23:2341–2348
53. Sastry GM, Adzhigirey M, Day T, Annabhimoju R, Sherman W (2013) Protein and ligand preparation: Parameters, protocols, and influence on virtual screening enrichments. J Comput Aid Mol Des 27(3):221–234
54. Schrödinger Release 2018–3: Schrödinger Suite 2018–3 Protein Preparation Wizard; Epik, Schrödinger, LLC, New York, NY, 2016 Impact, Schrödinger, LLC, New York, NY, 2016; Prime, Schrödinger, LLC, New York, NY, 2018; Schrödinger Release 2018–3: Prime, Schrödinger, LLC, New York, NY, 2018; Schrödinger Release 2018–3: MacroModel, Schrödinger, LLC, New York, NY, 2018; Schrödinger Release 2018–3: LigPrep Schrödinger LLC, New York, NY (2018)
55. Jacobson MP, Pincus DL, Rapp CS, Day TJF, Honig B, Shaw DE, Friesner RA (2004) A hierarchical approach to all-atom protein loop prediction. Proteins 55:351–367
56. Jacobson MP, Friesner RA, Xiang Z, Honig B (2002) On the role of crystal packing forces in determining protein side chain conformations. J Mol Biol 320:597–608
57. Schmidt MW, Baldridge KK, Boatz JA, Elbert ST, Gordon MS, Jensen JH, Koseki S, Matsunaga N, Nguyen KA, Su S, Windus TL, Dupuis M, Montgomery JA (1993) General atomic and molecular electronic structure system. J Comput Chem 14:1347–1363
58. Gordon MS, Schmidt MW (2005) In: Dykstra CE, Frenking G, Kim KS, Scuseria GE (eds) Theory and applications of computational chemistry: the first forty years. Elsevier, Amsterdam, pp 1167–1189
59. Ishikawa T, Kuwata K, Ishikawa T, Kuwata K (2009) Fragment molecular orbital calculation using the RI-MP2 method. Chem Phys Lett 474:195–198
60. Ishikawa T, Kuwata K (2012) RI-MP2 gradient calculation of large molecules using the fragment molecular orbital method. J Phys Chem Lett 3:375–379
61. Tomasi J, Mennucci B, Cammi R (2005) Quantum mechanical continuum solvation models. Chem Rev 105:2999–3093
62. Fedorov DG, Kitaura K, Li H, Jensen JH, Gordon MS (2006) The polarizable continuum model (PCM) interfaced with the fragment molecular orbital method (FMO). J Comput Chem 27:976–985
63. Li H, Fedorov DG, Nagata T, Kitaura K, Jensen JH, Gordon MS (2010) Energy gradients in combined fragment molecular orbital and polarizable continuum model (FMO/PCM) calculation. J Comput Chem 31:778–790
64. Fedorov DG, Kitaura K (2007) Pair interaction energy decomposition analysis. J Comput Chem 28:222–237
65. Tanaka S, Mochizuki Y, Komeiji Y, Okiyama Y, Fukuzawa K (2014) Electron-correlated fragment-molecular-orbital calculations for biomolecular and nano systems. Phys Chem Chem Phys 16:10310–10344
66. Ozawa M, Ozawa T, Ueda K (2017) Application of the fragment molecular orbital method analysis to fragment-based drug discovery of BET (bromodomain and extra-terminal proteins) inhibitors. J Mol Graphics Modell 74:73–82
67. https://www.moldiscovery.com/soft_grid.php. Accessed February 2019
68. Von Itzstein M, Wu W, Kok GB, Pegg MS, Dyason JC, Jin B, Phan TV, Smythe ML, White HF, Oliver SW, Colman PM, Varghese JN, Ryan DM, Woods JM, Bethell RC, Hotham VJ, Cameron JM, Penn CR (1993) Rational design of potent sialidase-based inhibitors of influenza virus replication. Nature 363:418–423
69. Milletti F, Storchi L, Sforna G, Cruciani G (2007) New and original pKa prediction method using grid molecular interaction fields. J Chem Inf Model 47:2172–2181
70. Milletti F, Storchi L, Sforna G, Cross S, Cruciani G (2009) Tautomer enumeration and stability prediction for virtual screening on large chemical databases. J Chem Inf Model 49:68–75
71. Ahlstrom MM, Ridderströ M, Luthman K, Zamora I (2005) Virtual screening and scaffold hopping based on GRID molecular interaction fields. J Chem Inf Model 45:1313–1323
72. Bergmann R, Linusson A, Zamora I (2007) SHOP: scaffold hopping by GRID-based similarity searches. J Med Chem 50:2708–2717
73. Pastor M, Cruciani G, McLay I, Pickett S, Clementi S (2000) Grid-independent descriptors (GRIND): a novel class of alignment-independent three-dimensional molecular descriptors. J Med Chem 43:3233–3243
74. Cruciani G, Carosati E, De Boeck B, Ethirajulu K, Mackie C, Howe T, Vianello R (2005) MetaSite: understanding metabolism in human cytochromes from the perspective of the chemist. J Med Chem 48:6970–6979
75. G. Cruciani (ed) Molecular Interaction Fields: Applications in drug discovery and ADME prediction, vol 27, Chapter 1. First published: 26 October 2005 Copyright © 2006 Wiley-VCH Verlag GmbH & Co. KGaA
76. G. van Rossum (1995) Python tutorial. Technical report CS-R9526, Centrum voor Wiskunde en Informatica (CWI), Amsterdam.
77. Heifetz A, Chudyk EI, Gleave L, Aldeghi M, Cherezov V, Fedorov DG, Biggin PC, Bodkin MJ (2016) The fragment molecular orbital method reveals new insight into the chemical nature of GPCR−ligand interactions. J Chem Inf Model 56:159–172
78. Fedorov DG, Kitaura K (2016) Subsystem analysis for the fragment molecular orbital method and its application to protein−ligand binding in solution. J Phys Chem A 120:2218–2231
79. Sunshine J, Taube JM (2015) PD-1/PD-L1 inhibitors. Curr Opin Pharmacol 23:32–38
80. Sun X, Liang L, Gu J, Zhuo W, Yan X, Xie T, Wu Z, Liu X, Gou X, Liu W, He G, Gan Y, Chang S, Shi H, Hu J (2019) Inhibition of programmed cell death protein ligand-1 (PD-L1) by benzyl ether derivatives: analyses of conformational change, molecular recognition and binding free energy. J Biomol Struct Dyn 37(18):4801–4812
81. Pascolutti R, Sun X, Kao J, Maute RL, Ring AM, Bowman GR, Kruse AC (2016) Structure and dynamics of PD-L1 and an ultra-high-affinity PD-1 receptor mutant. Structure 24:1719–1728
82. Shi D, Zhou S, Liu X, Zhao C, Liu H, Yao X (2018) Understanding the structural and energetic basis of PD-1 and monoclonal antibodies bound to PD-L1: a molecular modeling perspective. BBA General Subjects 1862:576–588
83. Ding H, Liu H (2019) Mapping the binding hot spots on human programmed cell death 1 and its ligand with free-energy simulations. J Chem Inf Model. https://doi.org/10.1021/acs.jcim.9b00337
84. Perry E, Mills JJ, Zhao B, Wang F, Sun Q, Christov PP, Tarr JC, Rietz TA, Olejniczak ET, Lee T, Fesik S (2019) Fragment-based screening of programmed death ligand 1 (PD-L1). Bioorg Med Chem Lett 29(6):786–790
85. Mejías C, Guirola O (2019) Pharmacophore model of immunocheckpoint protein PD-L1 by cosolvent molecular dynamics simulations. J Mol Graphics Modell 91:105–111

86. Eyrisch S, Helms V (2009) What induces pocket openings on protein surface patches involved in protein–protein interactions? J Comput Aid Mol Des 23:73–86
87. Guo W, Wisniewski JA, Ji H (2014) Hot spot-based design of small-molecule inhibitors for protein–protein interactions. Bioorg Med Chem Lett 24:2546–2554
88. Metz A, Pfleger C, Kopitz H, Pfeiffer-Marek S, Baringhaus K, Gohlke H (2011) Hot spots and transient pockets: predicting the determinants of small-molecule binding to a protein-protein interface. J Chem Inf Model 52:120–133
89. Stank A, Kokh DB, Fuller JC, Wade RC (2016) Protein binding pocket dynamics. Acc Chem Res 49:809–815